

Tug-of-war as a cooperative mechanism for bidirectional cargo transport by molecular motors

Melanie J. I. Müller*, Stefan Klump†, and Reinhard Lipowsky**

*Max Planck Institute of Colloids and Interfaces, Science Park Golm, 14424 Potsdam, Germany; and †Center for Theoretical Biological Physics, University of California at San Diego, La Jolla, CA 92093-0374

Edited by Charles S. Peskin, New York University, New York, NY and approved January 10, 2008 (received for review July 20, 2007)

Intracellular transport is based on molecular motors that pull cargos along cytoskeletal filaments. One motor species always moves in one direction, e.g., conventional kinesin moves to the microtubule plus end, whereas cytoplasmic dynein moves to the microtubule minus end. However, many cellular cargoes are observed to move bidirectionally, involving both plus- and minus-end-directed motors. The presumably simplest mechanism for such bidirectional transport is provided by a tug-of-war between the two motor species. This mechanism is studied theoretically using the load-dependent transport properties of individual motors as measured in single-molecule experiments. In contrast to previous expectations, such a tug-of-war is found to be highly cooperative and to exhibit seven different motility regimes depending on the precise values of the single motor parameters. The sensitivity of the transport process to small parameter changes can be used by the cell to regulate its cargo traffic.

bidirectional movement | cytoskeletal motor | intracellular transport | stochastic processes

The complex internal structure of biological cells depends to a large extent on targeted transport of vesicles, organelles, and other types of cargo. This active intracellular transport displays the counterintuitive property that many cargoes are observed to move bidirectionally, reversing direction every few seconds (1, 2). This “saltatory motion,” which is faster and more persistent than Brownian motion, has been known for a long time (3). With the improvement of experimental techniques, bidirectional motion has been found to be widespread, including particles such as mitochondria, pigment granules, endosomes, lipid-droplets, and viruses (2).

The long-range traffic inside biological cells is powered by molecular motors which transport cargos along microtubules (MTs). Some motors such as cytoplasmic dynein walk to the minus end, whereas others such as kinesin 1 or 2 walk to the plus end of the MTs. Cells often have a unidirectional MT cytoskeleton: The MT minus ends are typically located near the cell center, whereas the plus ends point outwards toward the cell periphery. Polarized cells like epithelial cells or axons possess a unipolar parallel MT array. Because of this unidirectional nature of the MT network and the motors, both plus and minus motors must be involved in the bidirectional transport of a single cargo. Indeed both kinesin and dynein are found simultaneously on various cellular cargoes (4–6). It is a matter of current research how the two motor species accomplish the bidirectional transport (1, 2, 7–9).

Two scenarios seem plausible (1, 2). (i) Tug-of-war: Each motor species tries to move the cargo into its own direction, thereby performing a “tug-of-war” on the cargo as depicted in Fig. 1. (ii) Coordination: An additional coordination complex prevents opposing motors from being active at the same time, thereby excluding state (0) in Fig. 1. In both cases, regulatory mechanisms, which may directly target the motors or the putative coordination complex, must be present to allow the cell to alter its motor transport in response to internal or external stimuli. The observed fast motion, and the complexity of bidi-

rectional transport, as briefly reviewed in the following paragraphs, has led many authors to reject a tug-of-war scenario and search for a coordination complex. However, as shown in this article, this rejection of the tug-of-war scenario is premature because a realistic tug-of-war leads to rather complex transport behavior that is not easily understood intuitively and, thus, may be erroneously interpreted as coordinated transport.

Most quantitative data have been obtained experimentally in two model systems: pigment granule transport in fish and frog melanophores (9–11) and lipid-droplet transport in *Drosophila* embryos (12–14). In melanophores, which are specialized pigment cells responsible for skin color, pigment granules move bidirectionally with similar velocities in both directions. They achieve net minus-end transport during an “aggregation period” because the average distance traveled in minus direction (the minus run length) is longer than the average distance traveled in plus direction (the plus run length). During a “dispersion period,” there is almost no net transport because of an increased minus run length (11).

Lipid droplets are storage organelles for lipids. In late *Drosophila* embryos, they move on a unipolar MT array in the egg periphery. Their bidirectional motion exhibits different patterns in different stages of embryonic development. In particular, from so-called phase II to III their net transport direction changes from plus to minus because of an increase in the minus run length (12, 14). This system is the only one for which force measurements have been performed so far. Stall forces have been found equal in plus and minus direction, independent of the net direction of droplet transport (12, 14).

Various proteins that are necessary for the proper function or regulation of motor transport have been identified (15). Examples are the dynein cofactor dynactin, which is necessary for bidirectional transport in melanophores (16), or various proteins like halo, klar, and LDS2 in the lipid droplet system (17).

Motor transport was found to be affected both by intracellular regulation and by mutational changes in the motor structure. First, cellular regulation often leads to changes in only one direction. In the lipid droplet system, net transport during embryogenesis is altered via a change in the plus run length (12), whereas in the melanophore system during skin color change, the minus run length is changed (11). Similarly, herpesvirus capsids achieve targeting during entry and egress by modulation of the plus run length (18). In all cases, the other direction is left unaltered. Second, mutation of the plus or minus motor mostly causes reduced motion in both directions by decreasing run

Author contributions: S.K. and R.L. designed research; M.J.I.M. performed research; and M.J.I.M. and R.L. wrote the paper.

The authors declare no conflict of interest.

This article is a PNAS Direct Submission.

Freely available online through the PNAS open access option.

*To whom correspondence should be addressed. E-mail: lipowsky@mpikg.mpg.de.

This article contains supporting information online at www.pnas.org/cgi/content/full/0706825105/DC1.

© 2008 by The National Academy of Sciences of the USA

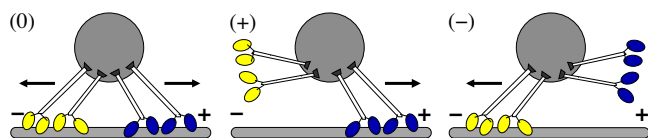


Fig. 1. Cargo transport by 2 plus (blue) and 2 minus (yellow) motors: possible configurations (0), (+), and (−) of motors bound to the MT. For configuration (0), the motors block each other so that the cargo does not move. For configuration (+) and (−), the cargo exhibits fast plus and minus motion, respectively.

lengths or velocities, as observed by mutating dynein on lipid-droplets (13, 14) and kinesin on axonal protein carrying vesicles (19). However, in melanophores, kinesin inactivation leads to breakdown of plus motion and increased minus run lengths (11).

Interfering with the dynein–cofactor dynactin impairs transport in both directions in melanophores (16), but impairs minus and enhances plus transport of adenovirus particles (20). In the only *in vitro* experiment concerning bidirectional transport (21), a motility assay of kinesin and dynein, it was observed that increasing the number of dyneins enhances minus and impairs plus end transport.

As shown here, all of these experimental observations are consistent with the tug-of-war mechanism. In fact, we present an explicit tug-of-war model that takes into account the experimentally known single motor properties and makes quantitative predictions for bidirectional transport. In our model, the motors act independently and interact only mechanically via their common cargo. We find seven possible motility regimes for cargo transport. Three of these regimes are dominated by the three configurations (0), (+), and (−) in Fig. 1 and represent no motion, fast plus motion, and fast minus motion of the cargo, respectively. The other motility states are combinations thereof; in particular, there are the two regimes, (−+) and (−0+), where the cargo displays fast bidirectional transport without and with pauses, respectively. During fast plus or minus motion, only one motor type is pulling most of the time and the tug-of-war appears to be coordinated.

The different motility regimes are found for certain ranges of single-motor parameters such as stall force and MT affinity. Small changes in these parameters lead to drastic changes in cargo transport, e.g., from fast plus motion to bidirectional motion or no motion. We propose that cells could use the sensitivity of the transport to the single-motor properties to regulate its traffic in a very efficient manner. We illustrate this general proposal by providing an explicit and quantitative tug-of-war model for the lipid-droplet system.

Results

Model. To study the bidirectional transport of cargos, we developed a model for a cargo to which N_+ plus and N_- minus motors are attached. Typically these numbers will be in the range of 1 to 10 motors as observed for many cargos *in vivo* (12, 22, 23). For $N_+ = 0$ or $N_- = 0$, we recover the model for cooperative transport by a single motor species as studied in ref. 24. We characterize each motor species by six parameters as measured in single molecule experiments [see Table 1 and supporting information (SI) Text] as follows: it binds to a MT with the binding rate π_0 and unbinds with the unbinding rate ε_0 , which increases exponentially under external force, with the force scale given by the detachment force F_d . When bound to the MT, the motor walks forward with the velocity v_F , which decreases with external force and reaches zero at the stall force F_s . Under superstall external forces, the motor walks backward slowly with backward velocity v_B .

The motors on the cargo bind to and unbind from a MT in a

Table 1. Values of the single-motor parameters for kinesin 1, cytoplasmic dynein, and an unknown plus motor (kin?) that transports *Drosophila* lipid droplets

Parameter	Kinesin 1	Dynein	kin?
Stall force F_s , pN	6 (29, 30)	1.1* (12, 27) 7 (31)	1.1* (12)
Detachment force F_d , pN	3 (30)	0.75*	0.82*
Unbinding rate ε_0 , s^{-1}	1 (30, 32)	0.27* (27, 33)	0.26*
Binding rate π_0 , s^{-1}	5 (34)	1.6* (33, 35)	1.6*
Forward velocity v_F , $\mu m/s$	1 (32, 36)	0.65* (33, 37)	0.55*
Back velocity v_B , nm/s	6 (36)	72*	67*

The kinesin 1 values have been taken from the cited references. The starred values are obtained by fitting experimental data of *Drosophila* lipid-droplet transport and are consistent with the cited references.

stochastic fashion, so that the cargo is pulled by $n_+ \leq N_+$ plus and $n_- \leq N_-$ minus motors, where n_+ and n_- fluctuate with time (see Fig. 2). We have derived the rates for unbinding of one of the bound motors and for binding of an additional motor on the cargo from the single motor rates under the assumption that: (i) the presence of opposing motors induces a load force, and (ii) this load force is shared equally by the bound motors belonging to the same species (see SI Text). We obtain a Master equation for the motor number probability $p(n_+, n_-)$ that the cargo is pulled by n_+ plus and n_- minus motors. The observable cargo motion is characterized by the motor states (n_+, n_-) with high probability. If there is high probability for a state $(n_+, 0)$ or $(0, n_-)$ with only one motor species bound, corresponding to Fig. 1(+), and (−), the cargo exhibits fast plus or minus motion, respectively. If there is high probability for a state with both motor species active, i.e., $n_+ > 0$ and $n_- > 0$, the cargo displays only negligible motion into the direction of the motors that “win” the tug-of-war, because the losing motors walk backward only very slowly. This corresponds to the blockade situation depicted in Fig. 1 (0).

Motility States for the Symmetric Case. We first studied the instructive symmetric case, for which the number of plus and minus motors are the same and where plus and minus motors have identical single-motor parameters except for their preferred direction of motion. Apart from being theoretically appealing, this symmetric situation can be realized *in vitro* if cargos are transported by a single motor species along antiparallel MT bundles, and can also be used *in vivo* provided plus and minus end transport exhibit sufficiently similar transport characteristics.

We solved our model for fixed motor numbers $N_+ = N_-$ and fixed single-motor parameters and determined the probability distribution $p(n_+, n_-)$ (see SI Text). Depending on the values of

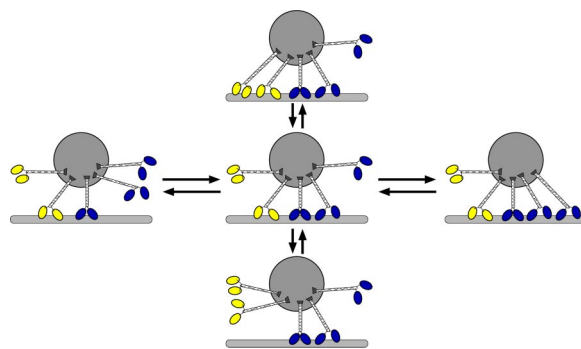


Fig. 2. A cargo with $N_+ = 3$ plus (blue) motors and $N_- = 2$ minus (yellow) motors is pulled by a fluctuating number of motors bound to the MT. The configuration in the middle corresponds to $(n_+, n_-) = (2, 1)$. Only five of 12 possible (n_+, n_-) configurations are displayed.

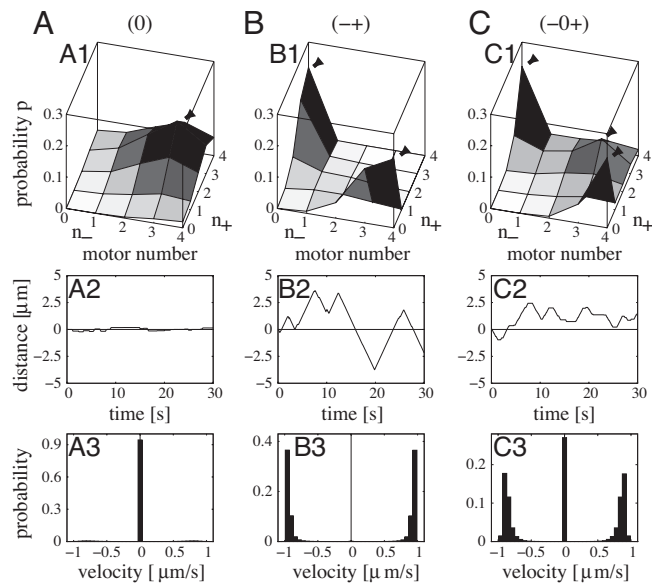


Fig. 3. Motility states for the symmetric tug-of-war of $N_+ = N_- = 4$ plus and minus motors. The three columns A, B, and C correspond to the three motility states (0), (-+), and (-0+), respectively. (A) The no-motion motility state (0) is characterized by motor number probabilities p with a single maximum at an equal number of active plus and minus motors (A1), trajectories with almost no motion (A2), and velocity distributions with a single maximum at zero velocity (A3). (B) The motility state (-+) of fast bidirectional motion is characterized by probabilities p with three maxima corresponding to fast plus and minus and no motion (B1), trajectories which exhibit switching between fast plus and minus motion (B2), and bimodal velocity distributions with two peaks close to the single-motor velocities of $\pm 1 \mu\text{m/s}$ (B3). (C) The motility state (-0+) is characterized by probabilities with three maxima corresponding to fast plus and minus and no motion (C1), trajectories that exhibit fast plus and minus motion and pauses (C2), and velocity distributions with three peaks (C3). Both plus and minus motors in B have the kinesin 1 parameters of Table 1. The different motility behavior in A and C is obtained by changing the single-motor parameters in Table 1 to (A) $F_s = 2 \text{ pN}$ and (C) $F_s = 4.75 \text{ pN}$ and $\varepsilon_0 = 0.4 \text{ s}^{-1}$.

these parameters, the model exhibits qualitatively different solutions (see Fig. 3), which we will call “motility states” in the following. These motility states exhibit distinct cargo trajectories and velocity distributions as shown in Fig. 3 and can formally be distinguished by the number of maxima of the motor number probability distribution $p(n_+, n_-)$. This number of maxima is found to be either 1, 2, or 3. For the symmetric case, three types of maxima with the configurations of Fig. 1 occur: a maximum with only plus and no minus motors bound (+), one with only minus and no plus motors bound (-), and one with equal numbers of plus and minus motors (0). These maxima are found in the combinations (0), (-+), and (-0+), leading to three qualitatively different motility states.

(0) No Motion. For “weak” motors with small stall to detachment force ratio $f = F_s/F_d$, the probability distribution $p(n_+, n_-)$ has a single maximum at a state with an equal number of bound plus and minus motors (see Fig. 3A1), and the velocity distribution has a peak at zero velocity (see Fig. 3A3). The corresponding cargo trajectories in Fig. 3A2 exhibit only small fluctuations around the initial position. This motility state (0) represents the blockade situation shown in Fig. 1 (0), which one naively expects for a tug-of-war scenario.

(-+) Fast Plus and Minus Motion. For strong motors with large f , cargo movement is completely different. The cargo switches between fast plus-directed and minus-directed motion (see Fig. 3B2) and the probability distribution $p(n_+, n_-)$ has two maxima

(see Fig. 3B1). At one maximum, only plus motors are bound to the MT ($n_+ > 0, n_- = 0$) and at the other only minus motors ($n_+ = 0, n_- > 0$), corresponding to the states (+) and (-) in Fig. 1, which are usually associated with coordinated transport rather than with a tug-of-war scenario. This behavior can be understood as follows: When more plus than minus motors are bound to the MT ($n_+ > n_-$), every plus motor experiences the force F_c/n_+ , whereas every minus motor experiences the larger force F_c/n_- , where F_c denotes the total force on the cargo. Because the unbinding rate increases strongly with increasing load force, minus motors are more likely to unbind from the MT than plus motors, so that the predominance of the plus motors is further enhanced. After the unbinding of a plus motor, the remaining minus motors experience an even larger force and are even more likely to unbind. As a consequence, the cargo experiences a cascade of minus motor unbinding events until no minus motor remains bound. A prerequisite for this unbinding cascade is that the motors can exert a sufficiently large force to pull off opposing motors from the MT, i.e., the stall force F_s has to be comparable or larger than the detachment force F_d . For small force ratios $f = F_s/F_d$, the pulling force has only a small effect on motor unbinding, so that no instability occurs and the cargo exhibits the blocked motility state (0). For large motor force ratio, the transient predominance of one motor type is thus amplified by a dynamic instability and most of the time only one motor type is bound, as indicated in Fig. 1(+ and -). The emergence of cooperative behavior arising from the nonlinear force-dependence of the unbinding rate has also been proposed as an explanation for collective effects in muscles (25) and mitotic spindle oscillations (26). For the tug-of-war of 4 against 4 motors with kinesin-like parameters as in Fig. 3B, $\approx 90\%$ of the time only one motor type is bound. During a plus or minus run, the effective velocity is slightly reduced compared with the single-motor velocity by the sporadic binding and subsequent fast unbinding of an opposing motor. The velocity distribution in Fig. 3B3 has two peaks close to the single-motor velocities $\pm 1 \mu\text{m/s}$. The direction of motion of the cargo is reversed when, due to a fluctuation, the defeated motors become predominant.

(-0+) Fast Plus and Minus Motion with Interspersed Pauses. Finally, in some intermediate parameter ranges, the probability distribution $p(n_+, n_-)$ exhibits three maxima as shown in Fig. 3C1, a symmetric one corresponding to no motion as for motility state (0) and two nonsymmetric ones corresponding to steady plus and minus motion as for state (-+). The velocity distribution has three corresponding peaks (see Fig. 3C3), and cargo trajectories therefore exhibit bidirectional motion interspersed with pauses (see Fig. 3C2).

Motility States for the Asymmetric Case. Bidirectional cargo transport *in vivo* is typically dependent on two different motor species for plus and minus motion. This plus-minus asymmetry can lead to net transport of the cargo in one direction. For example, in the motility state (-0+), the plus motion maximum (+) of the motor number probability can be larger than the minus motion maximum (-) (see Fig. 4A1), which leads to longer plus runs compared with minus runs and to net plus motion of the cargo as illustrated by the trajectory in Fig. 4A2. The velocity distribution in Fig. 4A3 has the three peaks characteristic for the (-0+) regime, but the peak at high plus velocity is larger than the one at high minus velocity. Because cargo motion is no longer symmetric with respect to plus and minus motion, seven motility states are now possible, corresponding to the different combinations (+), (-), (0), (-+), (0+), (-0) and (-0+) of the maxima (+), (-), and (0). The new motility states (0+) and (-0) are shown in Fig. 4B and C. The two other new states (-0) and (-) are analogous with plus and minus motion interchanged.

In the motility state (0+), the motor number probability has a

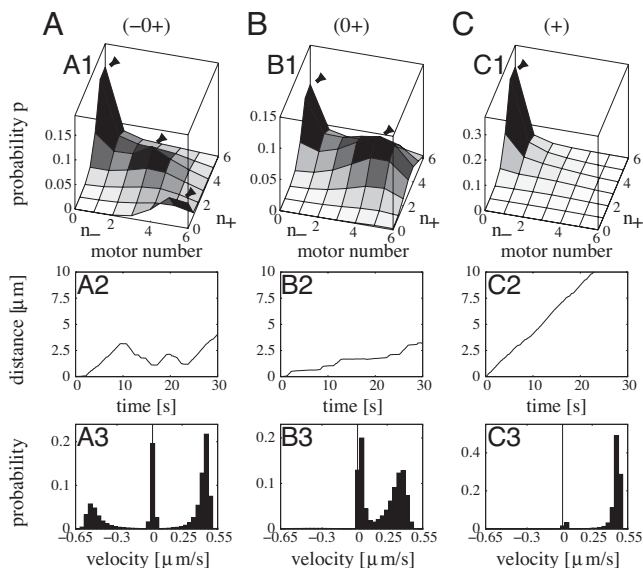


Fig. 4. Motility states for the asymmetric tug-of-war of $N_+ = 6$ plus against $N_- = 6$ minus motors. The cargo is in one of seven motility states. The motility states (0), (-+) and (-0+) are as for the symmetric case shown in Fig. 3, except that the plus-minus symmetry is lost as illustrated in A for the (-0+) motility state. (A) The (-0+) is characterized by three maxima in the motor number probability p at a plus, a minus, and a no-motion state (A1), trajectories with rapid plus and minus motion interspersed with pauses (A2), and three peaks in the velocity distribution (A3). Plus motion has a higher probability so that net motion is plus-end directed. (B) The (0+) motility state is characterized by probabilities p with one maximum with only plus motors and one with plus and minus motors active (B1), trajectories with fast plus motion and pauses (B2), and velocity distributions with two peaks near the single plus motor velocity $v_{F+} = 0.55 \mu\text{m/s}$ and near zero. (C) The (+) motility state is characterized by probabilities p with a maximum with only plus motors active (C1), trajectories with fast plus motion (C2), and velocity distributions with a peak close to the single plus motor velocity (C3). The motility states (-0) are similar to the states (0+) and (+) with plus and minus interchanged. A represents lipid-droplet transport: The plus and minus motors have the *Drosophila* plus motor (kin?) and dynein parameters of Table 1. The same parameters are used in B and C except for $F_{s-} = 0.45 \text{ pN}$ (B and C), $\varepsilon_{0-} = 0.24 \text{ s}^{-1}$ (B), and $\varepsilon_{0-} = 0.54 \text{ s}^{-1}$ (C).

maximum at the plus motion state (+) with only plus motors active and a maximum at the no-motion state (0) with both types of motors active (see Fig. 4B1). The corresponding velocity distribution in Fig. 4B3 has two peaks, one close to zero velocity and one at large plus motor velocity, and the cargo switches between fast plus motion and pauses (see Fig. 4B2). In the (+) motility state in Fig. 4C, the motor number probability and velocity distribution exhibit a maximum corresponding to fast plus motion. [The small peak near zero velocity corresponds to the no-motion states near the maximum for which both n_+ and n_- are non-zero.]

In Vivo Tug-of-War. To check whether our model can account quantitatively for experimental observations, we applied our model to the bidirectional movements of lipid droplets in *Drosophila* embryos. We chose this particular series of sophisticated experiments (12–14) because it is unique in providing an estimate for the number of motors on the cargo, a high number of quantitative measurements of transport characteristics including cargo force measurements, as well as observations in two different developmental phases (labeled wild-type phase II and III, WT II and WT III) and in three different dynein mutation backgrounds. The droplets are transported by an unknown plus motor, presumably an unconventional kinesin, and cytoplasmic dynein (13).

We first considered the WT II data. Cargo stall force measurements led to the conclusion that the droplets are on average

pulled by 5 plus and 5 minus motors, and that both types of motors have a single-motor stall force of 1.1 pN (12). Because the number of active motors fluctuates stochastically, this should be the average number of pulling motors. Therefore, we fixed the total number of plus and minus motors to $N_+ = N_- = 6$.

We then performed simulations and varied the undetermined single motor parameters to fit the experimentally measured transport characteristics, namely plus and minus run lengths, plus and minus stall forces, pause times after plus and minus travel, and plus and minus velocities of short and long runs, with an accuracy of $\approx 10\%$ (for the detailed procedure and results of this and the following fits see *SI Text* and *SI Tables 2 and 3*). The resulting parameters for dynein and the unknown plus motor (kin?) are listed in Table 1. The dynein parameters are in agreement with *in vitro* measurements of dynein properties when available. All other parameter lie in a reasonable range. The dynein backward velocity is an order of magnitude larger than for kinesin 1, in agreement with experiments (27, 28).

Fig. 4A shows a sample trajectory, the motor number probability, and the velocity distribution for the droplet tug-of-war in WT II. The cargo switches between fast plus and minus motion and pauses but exhibits net plus motion because the probability for (+) states is higher than for (-) states. The cargo stall forces in plus and minus direction are equal (see *SI Table 3*). This shows that the cargo direction is not only determined by the motor forces but also by other motor properties (see Table 1). In this case, the higher plus motor detachment force makes it difficult to rip off the plus motors and thus favors plus motion.

A nontrivial consistency check of our model is provided by three additional features that we obtained from this model in close agreement with experimental observations even though these features were not used to determine the model parameters in Table 1. First, the distribution of plus and minus run lengths can be fitted by a sum of two exponentials (this has also been found in the melanophore system; ref. 11) with length scales of the same order of magnitude as obtained experimentally (14) (see Fig. 5A). Second, the pause time distributions of pauses after plus and after minus runs are very similar and can be fitted by a single exponential function with a time scale of the same order of magnitude as in the experiments (13) (see *SI Fig. 11*). Third, there is a correlation between run length and run velocity: long runs have larger average velocities (see Fig. 5B). In the experiments (13, 14), this has been quantified by dividing the runs into short runs ($0.03\text{--}0.1 \mu\text{m}$) and long runs ($0.5\text{--}1 \mu\text{m}$). Short runs have approximately half the velocity of long runs (see Fig. 5C). In our model, this property reflects the correlation of the average number of active winning motors with the run length (see *SI Fig. 8*) and can be understood as follows.

During a certain run, e.g., in the plus direction, minus motors bind from time to time to the MT. This slows down the motion and causes a “pause.” However, the active plus motors generate a large force on this single minus motor, which is then ripped off fast from the MT. As a consequence, the pauses are too short to be detected experimentally and are only noticeable via the decreased average cargo velocity in the plus direction. If a cargo is pulled by many plus motors, this has two effects: (i) The effective cargo velocity is increased because opposing minus motors do not create large forces on each of the many plus motors and because the minus motor drops off very fast. (ii) The plus run length is larger because it is less probable that the minus motors take over. Both effects together lead to a correlation of run length and velocity.

Mutation and Regulation. Three different dynein mutations in *Drosophila* embryos of developmental phase II have been studied (13, 14), and all three lead to impairment of both plus and minus motion with reduced run lengths and stall forces. At first sight, this simultaneous impairment of both transport directions in response to mutations that affect only one of the two motor

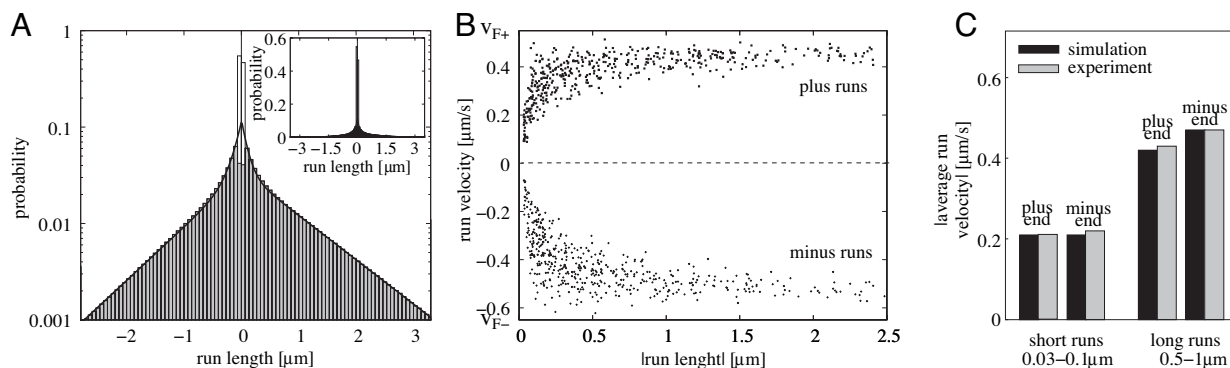


Fig. 5. *Drosophila* lipid-droplet transport in wild type phase II: tug-of-war of six *Drosophila* plus motors and six dyneins with parameters as in Table 1. (A) Distribution of run length, the distance traveled in one direction before a pause or a directional switch occurs. Minus (plus) run lengths are negative (positive). The gray bars are the run lengths observable with the experimental cutoffs of a minimum length of 0.16 s and 30 nm, whereas the white bars are obtained without the cutoffs and thus beyond experimental resolution. The lines are double exponential fits to the simulation data with decay lengths of $\approx 0.1 \mu\text{m}$ and $1 \mu\text{m}$ in both directions, of the same order of magnitude as in the experiments (14). (B) Scatter plot of the run velocity (positive for plus and negative for minus runs) versus the run length of 500 runs in each direction shows a positive correlation: longer runs have higher velocities. The Spearman rank correlation coefficient both for plus and minus motion is >0.7 with a significance level below 10^{-10} . Long runs have almost the maximal velocity which is the single motor velocity, v_{F+} in plus and $-v_{F-}$ in minus direction. There are no data points for small run lengths and velocities because runs have been defined as periods with a velocity larger than 50 nm/s for at least 30 nm. (C) The correlation of run length and velocity can also be seen by considering short (0.03–0.1 μm) and long (0.5–1 μm) plus and minus end runs, respectively. Short runs have lower averages than long runs, which reproduces the experimental averages of ref. 14.

species seems to be inconsistent with a tug-of-war. However, using our tug-of-war model, we were again able to describe the observed behavior with an accuracy of $\approx 10\%$. To do so, we only varied the minus motor parameters and kept the plus motor parameters fixed to their WT II values (see SI Table 3).

In our model, the dynein mutations simultaneously modify several parameters of this motor, among which are its unbinding rate, its binding rate, and its detachment force. If only one of these parameters were modified, the resulting motor behavior would be easy to understand. First, if only the unbinding rate is increased, the minus motors unbind from the filament faster and thus produce less force on the plus motors, which leads to longer plus and shorter minus runs. Second, increasing only the minus motor binding rate has the opposite effect because dyneins are more likely to rebind to the filament. Third, if only the minus motor detachment force is enhanced, the ability of the minus motors to resist the plus motors is also enhanced, which increases minus and decreases plus run lengths. Therefore, if only a single parameter of the minus motor is modified, motion in one direction is enhanced whereas motion in the opposite direction is impaired. On the other hand, the overall effect of changes in several motor parameters is difficult to anticipate intuitively and can lead to impairment of both directions as shown in our model.

Furthermore, two different embryonic phases WT II and WT III allow to assess the effect of cellular regulation. In WT II, net droplet transport is plus-end directed, whereas it is minus-end directed in WT III due to a reduction in plus run lengths. Apart from the stall forces, all other transport characteristics remain unchanged. We propose that the cellular regulation that causes this change targets the motor properties. Therefore, we fitted the WT III data by varying the single-motor parameters as for the WT II data. The fit shows that a tug-of-war can lead to impairment of motion in one direction while leaving the other direction unaffected (see SI Table 3). The obtained single-motor parameters for WT II and WT III are rather similar. This sensitivity of motion to the single-motor parameters allows the cell to regulate its transport in an efficient way.

In the only *in vitro* experiment concerning bidirectional transport (21), a motility assay of kinesin and dynein, it was observed that increasing the number of transporting dyneins enhances

minus and impairs plus end transport. This is reproduced in our model (compare SI Table 3).

Discussion

We have investigated a model for bidirectional cargo transport based on a tug-of-war between plus and minus motors governed by mechanical interactions only. Our model exhibits many features that are usually attributed to a coordination mechanism. In particular, even for equally strong motors, a tug-of-war does not necessarily lead to the expected blockade situation with almost no cargo motion as in Fig. 1 (0), but can also lead to switching between fast plus end and fast minus end motion as in Fig. 1 (+) and (–). This surprising behavior is caused by a dynamic instability arising from the strongly nonlinear force-dependence of the single-motor unbinding rate. This instability leads to a high probability of having only one motor type active at a given time.

In our tug-of-war model, the motility behavior of the cargo is very sensitive to the single-motor properties. Changing the motor stall force or MT affinity, for example, can lead to qualitatively different motility behavior such as fast plus motion, no motion, or bidirectional transport. When we modified the single-motor properties to mimic the effect of either mutations or of regulatory processes, we found that motion in plus and minus direction can be affected in various ways. We found cases for which (i) motion was affected only in one direction, (ii) motion was impaired in one direction and enhanced in the other, and (iii) motion was enhanced or impaired in both directions. This variability agrees with experimental observations where different systems also exhibit widely varying reactions to regulation or mutation (11–14, 16, 18–20) as described in the Introduction.

Our tug-of-war model is thus in qualitative agreement with experimental data for bidirectional transport *in vivo*. Furthermore, we have been able to quantitatively describe the experimental data for the *Drosophila* lipid droplet system. The latter system exhibits different transport regimes depending (i) on the different phases of the embryonic development, which are distinguished by distinct sets of regulatory proteins, and (ii) on the molecular structure of the motor proteins, which have been changed by mutations. In our theory, these different transport regimes arise from variations in single-motor parameters, but the basic transport mechanism underlying all of

these regimes is provided by a tug-of-war between the two motor species.

Our results show that the two scenarios for bidirectional transport displayed in Fig. 1, namely the tug-of-war and coordinated motor activity, are not mutually exclusive, but rather that the tug-of-war provides a mechanism for coordinated movement.

1. Gross SP (2004) *Phys Biol* 1:R1–R11.
2. Welte MA (2004) *Curr Biol* 14:R525–R537.
3. Rebhun L (1967) *J Gen Physiol* 50:223–239.
4. Rogers SL, Tint IS, Fanapour PC, Gelfand VI (1997) *Proc Natl Acad Sci USA* 94:3720–3725.
5. Ligon LA, Tokito M, Finklestein JM, Grossmann FE, Holzbaur ELF (2004) *J Biol Chem* 279:19201–19208.
6. Pilling AD, Horiuchi D, Lively CM, Saxton WM (2006) *Mol Biol Cell* 17:2057–2068.
7. Kural C, Kim H, Syed S, Goshima G, Gelfand V, Selvin PR (2005) *Science* 308:1469–491.
8. Gennerich A, Schild D (2006) *Phys Biol* 3:45–53.
9. Levi V, Serpinskaya AS, Gratton E, Gelfand VI (2006) *J Cell Biol* 90:318–327.
10. Nascimento AA, Roland JT, Gelfand VI (2003) *Annu Rev Cell Dev Biol* 19:469–491.
11. Gross SP, Tuma MC, Deacon SW, Serpinskaya AS, Reilein AR, Gelfand VI (2002) *J Cell Biol* 156:855–865.
12. Welte MA, Gross SP, Postner M, Block SM, Wieschaus EF (1998) *Cell* 92:547–557.
13. Gross SP, Welte MA, Block SM, Wieschaus EF (2000) *J Cell Biol* 148:945–955.
14. Gross SP, Welt MA, Block SM, Wieschaus EF (2002) *J Cell Biol* 156:715–724.
15. Reilein AR, Rogers SL, Tuma MC, Gelfand VI (2001) *Int Rev Cytol* 204:179–238.
16. Deacon SW, Serpinskaya AS, Vaughan PS, Fanarraga ML, Vernos I, Vaughan KT, Gelfand VI (2003) *J Cell Biol* 160:297–301.
17. Welte MA, Cermelli S, Griner J, Viera A, Guo Y, Kim DH, Gindhart JG, Gross SP (2005) *Curr Biol* 15:1266–1275.
18. Smith GA, Murphy BJ, Gross SP, Enquist LW (2004) *Proc Natl Acad Sci USA* 101:16034–16039.
19. Kaether C, Skehel P, Dotti CG (2000) *Mol Biol Cell* 11:1213–1224.
20. Suomalainen M, Nakano MY, Keller S, Boucke K, Stidwill RP, Greber UF (1999) *J Cell Biol* 144:657–672.
21. Vale RD, Malik F, Brown D (1992) *J Cell Biol* 119:1589–1596.
22. Ashkin A, Schütze K, Dziedzic JM, Euteneuer U, Schliwa M (1990) *Nature* 348:346–348.
23. Blocker A, Serevin FF, Burkhardt JK, Bingham JB, Yu H, Olivo JC, Schroer TA, Hyman AA, Griffiths G (1997) *J Cell Biol* 137:113–129.
24. Klumpp S, Lipowsky R (2005) *Proc Natl Acad Sci USA* 102:17284–17289.
25. Duke T (2000) *Phil Trans R Soc Lond B* 355:529–538.
26. Grill S, Kruse K, Jülicher F (2005) *Phys Rev Lett* 94:108104.
27. Mallik R, Petrov D, Lex SA, King SJ, Gross SP (2005) *Nature* 427:649–652.
28. Wang Z, Khan S, Sheetz MP (1995) *Biophys J* 69:2011–2023.
29. Svoboda K, Block SM (1994) *Cell* 77:773–784.
30. Schnitzer MJ, Visscher K, Block SM (2000) *Nat Cell Biol* 2:718–723.
31. Toba S, Watanabe TM, Yamaguchi-Okimoto L, Toyoshima YY, Higuchi H (2006) *Proc Natl Acad Sci USA* 103:5741–5745.
32. Vale RD, Funatsu TS, Pierce DW, Romberg L, Harada Y, Yanagida T (1996) *Nature* 380:451–453.
33. King SJ, Schroer TA (2000) *Nat Cell Biol* 2:20–24.
34. Leduc C, Campas O, Zeldovich KB, Roux A, Jolimaître P, Bourel-Bonnet L, Goud B, Joanny J-F, Bassereau P, Prost J (2004) *Proc Natl Acad Sci USA* 101:17096–17101.
35. Reck-Peterson SL, Yildiz A, Carter AP, Gennerich A, Zhang N, Vale RD (2006) *Cell* 126:335–348.
36. Carter NJ, Cross RA (2005) *Nature* 435:308–312.
37. Nishiura M, Kon T, Shiroguchi K, Ohkura R, Shima T, Toyoshima YY, Sutoh K (2004) *J Biol Chem* 279:22799–22802.

ACKNOWLEDGMENTS. We thank Cécile Leduc for pointing out a problem in a previous version of our model. M.J.I.M. was supported by the European Commission Sixth Framework Programme [Specific Targeted Research Project (STREP) Contract No. NMP4-CT-2004-516989]. S.K. was supported by Deutsche Forschungsgemeinschaft Grants KL818/1–1 and 1–2 and by the National Science Foundation through the Physics Frontiers Center-sponsored Center for Theoretical Biological Physics (Grants PHY-0216576 and PHY-0225630).